



# Lawrence Berkeley Laboratory

UNIVERSITY OF CALIFORNIA

RECEIVED  
LAWRENCE  
BERKELEY LABORATORY  
NOV 1 1984  
LIBRARY AND  
DOCUMENTS SECTION

## Materials & Molecular Research Division

Presented, in part, at the Meeting of the  
Electrochemical Society, San Francisco, CA,  
May 8-13, 1983; and submitted to the Journal  
of the Electrochemical Society

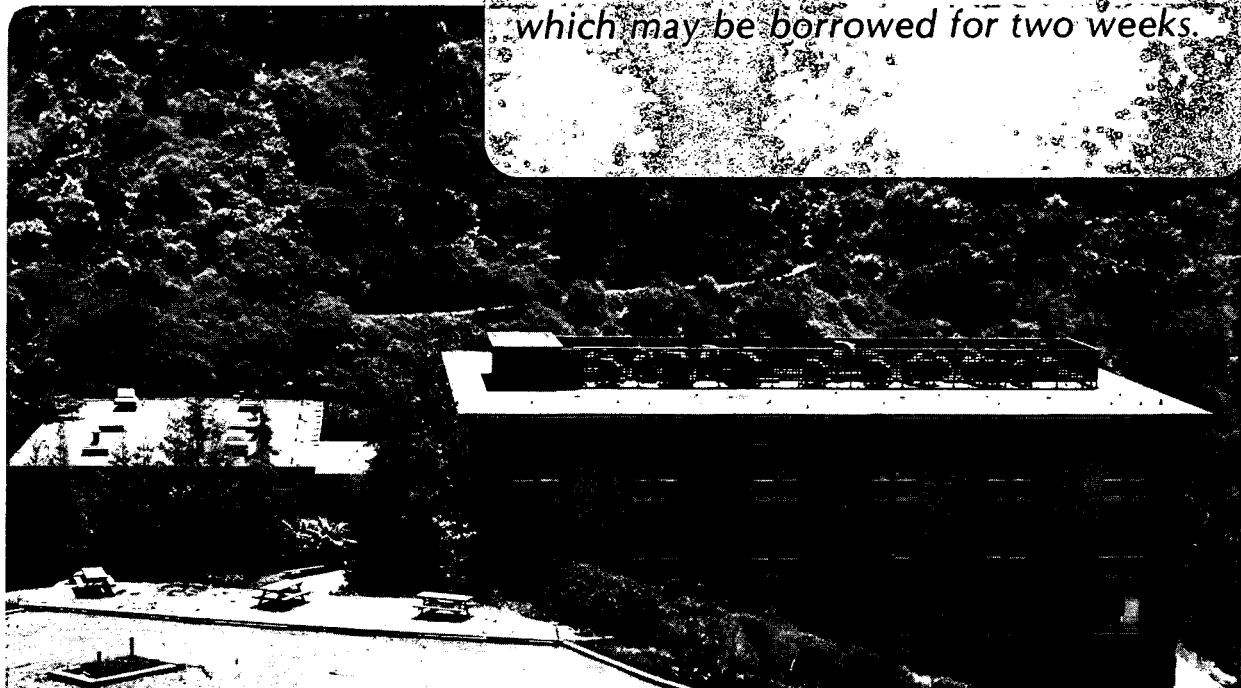
EFFECT OF RHODAMINE-B ON THE ELECTRODEPOSITION  
OF LEAD ON COPPER

J.C. Farmer and R.H. Muller

September 1984

**TWO-WEEK LOAN COPY**

*This is a Library Circulating Copy  
which may be borrowed for two weeks.*



LBL-17014 Rev. c.2

## **DISCLAIMER**

This document was prepared as an account of work sponsored by the United States Government. While this document is believed to contain correct information, neither the United States Government nor any agency thereof, nor the Regents of the University of California, nor any of their employees, makes any warranty, express or implied, or assumes any legal responsibility for the accuracy, completeness, or usefulness of any information, apparatus, product, or process disclosed, or represents that its use would not infringe privately owned rights. Reference herein to any specific commercial product, process, or service by its trade name, trademark, manufacturer, or otherwise, does not necessarily constitute or imply its endorsement, recommendation, or favoring by the United States Government or any agency thereof, or the Regents of the University of California. The views and opinions of authors expressed herein do not necessarily state or reflect those of the United States Government or any agency thereof or the Regents of the University of California.

EFFECT OF RHODAMINE-B ON THE ELECTRODEPOSITION  
OF LEAD ON COPPER

Joseph C. Farmer\* and Rolf H. Muller

Materials and Molecular Research Division  
Lawrence Berkeley Laboratory  
and  
Department of Chemical Engineering  
University of California, Berkeley  
Berkeley, California 94720

\*Present address: Sandia Laboratory, Livermore, CA 94550

## ABSTRACT

Rhodamine-B chloride (10 $\mu$ M) has been used as a model plating additive in a study of the electrodeposition of Pb from 1 M NaClO<sub>4</sub>, 0.5 and 5 mM Pb<sup>++</sup> (pH 3) on Cu. Ellipsometer measurements during cyclic voltammetry have shown that the addition of dye results in a more compact bulk deposit than obtained in its absence. It also prevents complete monolayer coverage during formation of the Pb underpotential deposit and shifts the bulk deposition peak to more cathodic potentials during the first potential cycle. Dye effects on potential and micromorphology disappear during subsequent cycling, but reappear after relaxation periods at open circuit. Depletion and readsorption of dye on the surface have been confirmed by spectroscopic ellipsometry. Different optical film models have been investigated for the interpretation of spectroscopic ellipsometer measurements by use of multidimensional analysis.

Surface active agents (additives, inhibitors) have long been used on an empirical basis to control surface finish in electrolytic metal deposition and indications are that uncontrolled impurities often cause similar effects. Few fundamental studies have been undertaken to define the role of these agents during the initial stages of electrocrystallization, despite the great technical importance of their use (1). The objectives of this work were to correlate variations in adsorbate coverage on the electrode with differences in overpotential and micromorphology of the deposit. Deposit thicknesses investigated ranged from a monolayer (the underpotential deposit, UPD) to thicknesses of about 100 nm. The principal experimental techniques used were cyclic voltammetry and ellipsometry (both spectroscopic and fixed-wavelength). A self-compensating instrument with rapid spectral scanning capabilities for the visible range and automated data collection has been built for this purpose and is discussed elsewhere (2, 3).

### I. Selection of Electrochemical System

The materials used in this study were selected to satisfy electrochemical and optical criteria. Most of the experimental investigations were conducted with Cu as the electrode substrate, Pb as the deposited metal, and Rhodamine-B chloride as the model inhibitor. The supporting electrolyte was composed of 1 molar sodium perchlorate, acidified to a pH of 3 by use of perchloric acid. The inhibitor concentration was typically 10 micromolar and  $Pb^{++}$  ion concentration was 5.0 millimolar (as nitrate).

The materials chosen have optical constants which are distinguishable over the spectral range accessible to the optical instrumentation (370 to 720 nm): Cu shows a distinctive absorption in the visible (around 550 nm), which is

believed to be due to electronic transitions from the filled d bands into the sp conduction bands (4-6). In contrast to Cu, Pb shows no such characteristic in the visible and has relatively flat optical constants (7). Dissolved Rhodamine-B has a characteristic absorption band at about 555 nm, believed to be due to an electronic transition from a singlet ground state to an excited triplet state (8). The electronic transition moment related to this absorption process lies parallel to the three conjugated rings of the Rhodamine-B molecule. Rhodamine-B can be expected to adsorb on the surface with a preferential orientation of the transition moment, resulting in a birefringent (dichroic) adsorbate layer. This birefringence, and its spectral dependence, can be interpreted in terms of molecular orientation of the adsorbate on the surface (9, 10).

Electrochemically, Cu is stable to dissolution and oxidation at the reversible potential for Pb deposition from acidic solutions (11) and Pb forms a well-defined underpotential deposit on Cu substrates (12). In screening studies with over 30 materials, 14 of which were indicators or laser dyes, Rhodamine-B was found to induce the largest increase in overpotential (125 mV) for bulk Pb deposition.

## II. Experimental Procedure

The automatic spectroscopic ellipsometer used in this study employed the polarizer-compensator-sample-analyzer optical configuration. It was self-nulling by use of a magneto-optic polarizer and analyzer, and could be operated in either a spectroscopic or fixed wavelength mode (2, 3). The spectral range was 370 nm to 720 nm, the angle-of-incidence used was 75 degrees. A complete scan of spectroscopic measurements ( $\Delta$  and  $\Psi$  at different wavelengths) could be made in 3 seconds, although improved signal-to-noise ratios

were obtained with slower scanning (e.g., one scan per 15 seconds) or by averaging multiple scans. Slower scanning was essential to observe dye adsorption whereas faster scanning gave sufficient signal quality for resolution of deposit micromorphology. Data acquisition was fully automated with a LSI-11/02 microcomputer system, which was also used for instrument calibrations and to interpret measurements by use of optical models.

The electrochemical cell used for experiments with Cu substrates was made of Teflon. It was designed for clean operation and low light absorption in the solution with a small liquid volume (2 ml) and a short optical path (2.5 cm) through the solution. The cell was pie-shaped, with windows made of polished and annealed optical quality quartz, oriented normal to incident and reflected light beams for operation at an angle of incidence of 75 deg.

The round working electrodes were machined from polycrystalline oxygen-free Cu with an exposed surface of 1.27 cm diam. The electrodes were polished mechanically with a final alumina abrasive of 0.05 micron. Air-formed oxide on the electrode surface was removed by prepolarization in the acidic electrolyte. The counter electrode consisted of a Pb wire (99.999% purity) wound into a flat spiral, positioned 0.8 cm from the working electrode and of equal diameter. Lead oxide resulting from the corrosion of the counter electrode was removed by cathodic pre-polarization, using a second Pb wire electrode and an initial electrolyte charge. The initial electrolyte charge was replaced when the Cu working electrode was inserted, without exposing the anode to air.

A double-junction Ag/AgCl reference electrode (Dow-Corning 476067), inserted into a Teflon reference electrode compartment, was connected to the electrochemical cell with a Teflon capillary (0.16 cm o.d.). The reference electrode was connected to the potentiostat via an electrometer probe (PAR).

Two syringes (15 ml each) were used to supply electrolyte to and withdraw from the cell. The electrolyte consisted of 5 mM  $\text{Pb}(\text{NO}_3)_2$ , 1 M  $\text{NaClO}_4$  at pH 3, with or without 10 $\mu\text{M}$  Rhodamine-B addition. It was prepared from deionized, singly distilled (10 megohm) water and analytical grade salts. The electrolyte was nitrogen-stripped for about 15 minutes prior to experiments, and the cell was purged with nitrogen before filling. The syringes and a nitrogen purge stream were connected with Teflon capillaries.

The potential of the working electrode was controlled with a potentiostat (PAR 173) and the charge passed was determined with a digital coulometer (PAR 179). The coulombic efficiencies between deposition and dissolution were always greater than 95%. Film thickness  $d_q$  based on charge is that given for a compact lead layer. Cell potential and current, together with the measured ellipsometer parameters  $\Delta$  and  $\psi$  (measured as Faraday cell currents), were recorded by the LSI microcomputer system via an 8-channel analog-to-digital converter (Data1 MST-LSI2).

### III. Spectroscopic Ellipsometry

#### 1. Electrochemical Deposition of Pb Films

Thin films of lead on copper substrates were prepared by potentiostatic deposition (-600 mV vs. Ag/AgCl) from an electrolyte consisting of 5 mM  $\text{Pb}(\text{NO}_3)_2$  and 1 M  $\text{NaClO}_4$  at a pH of 3, with deposition times of 1-8 min.

Based upon charge passed, the film thicknesses  $d_q$  would have been 31, 60 and 110 nm if the deposit had formed uniformly and had been compact. However, it was found that the deposit was not homogeneous and compact, and multilayer optical models had to be used to explain the spectroscopic ellipsometer measurements.

## 2. Single-Layer Optical Models

Film models investigated for the interpretation of measurements are illustrated in Fig. 1 (2). Examples of interpretations given below illustrate the use of the high information content of spectroscopic ellipsometer measurements from the derivation of wavelength-independent film parameters. Predictions based upon the following three optical models for single layer films (Fig. 1a-c) are compared to experimental spectroscopic ellipsometer measurements in Figs. 2-4. In the compact film model, the entire deposit was treated as bulk Pb and there was only one adjustable parameter, the deposit thickness. Figure 4 shows spectroscopic simulations of  $\Delta$  for various assumed thicknesses (solid lines labeled 0, 1, 5, 10 nm, etc.). Comparison with experimental measurements also shown on the figure (dotted lines for 31, 60, and 110 nm compact thicknesses) illustrates that this model is inadequate.

The second single-layer optical model was that of a porous film in which porosity was taken into consideration by use of an effective refractive index. Pores were treated as microinclusions of electrolyte ( $n=1.34$ ) in a Pb host medium ( $\hat{n}=2.1-4.2i$ ) and the optical properties of an isotropic homogenous film were computed by use of the Maxwell-Garnett or Bruggeman equations. These equations have been used in the literature for modeling rough surfaces and particulate films (13-16). This model involved two adjustable parameters, the deposit thickness and porosity. Spectroscopic simulations of the ellipsometer parameter  $\Delta$  for this model are shown in Fig. 3 for an amount of deposit corresponding to a 31 nm thick, compact Pb layer (based upon coulometric measurements) redistributed on a Cu substrate as deposits of various porosities. Simulations are represented by solid lines and experi-

mental measurements are represented by dotted lines. It is evident that this model alone is also inadequate to explain experimental measurements of delta and deposit thickness based on charge.

The third model was based on the coherent superposition of polarization states resulting from reflection of adjacent film-covered and bare elements of a patchwise covered surface ( 17-19 ). The island film may be compact, porous or anisotropic. In the latter case, at least six unknown film parameters would have to be determined, which results in unacceptable parameter variances. The dimensions of the islands are assumed to be smaller than the transverse and longitudinal coherence of the incident light at the specimen surface. For the present spectroscopic ellipsometer, the longitudinal coherence ranges from  $16\ \mu\text{m}$  at 400 nm to  $49\ \mu\text{m}$  at 700 nm (20); the transverse (lateral) coherence ranges from  $10\ \mu\text{m}$  at 400 nm to  $17\ \mu\text{m}$  at 700 nm (21). These estimates assume (conservatively) a bandwidth twice that of the source (20 nm). Since complementary SEM studies of the films investigated here have shown the dimensions of dendritic islands to be less than  $15\ \mu\text{m}$  use of the coherent superposition model is justified for the present experiments.

Spectroscopic simulations of delta for films corresponding to a 31 nm thick, uniform, compact Pb deposit (based upon coulometric measurements), redistributed on a Cu substrate as compact islands, are shown in Fig. 4. The island model used for these simulations employed two

adjustable parameters, fractional surface coverage and island thickness. Combinations of these two parameters which were consistent with the amount of Pb known to be in the film from coulometric measurements were used. It can be seen that this model is also incapable of explaining the experimental measurements.

For all single-layer optical models, disagreement of the computed spectral dependence of psi was similar to that shown for delta. It is important to note that interpretations of measurements at a single wavelength often are possible, but the entire spectral range cannot be fitted with any of the models. This fact illustrates the greatly increased information content of spectroscopic measurements.

### 3. Multiple-Layer Optical Models

A three-layer model (2) is illustrated in Fig. 1d. The first layer was assumed to be an isotropic film representing the underpotential deposit. Optical properties of this layer were determined in a separate study (22).

The second layer was assumed to be a granular, porous deposit with optical constants computed from the properties of Pb and electrolyte, by use of the Bruggeman theory for a binary mixture, Eqs. 1-5. Incorporation of this layer into the optical model was motivated by light scattering measurements (22).

$$\frac{\hat{\epsilon}_{\text{Pb}} - \hat{\epsilon}_f}{\hat{\epsilon}_{\text{Pb}} + 2\hat{\epsilon}_f} \theta_{\text{Pb}} + \frac{\hat{\epsilon}_s - \hat{\epsilon}_f}{\hat{\epsilon}_s + 2\hat{\epsilon}_f} (1 - \theta_{\text{Pb}}) = 0 \quad (1)$$

$$\hat{\epsilon}_f = \frac{1}{2} [-\hat{A} \pm (\hat{A}^2 - 4\hat{B})^{1/2}] \quad (2)$$

$$\hat{A} = \frac{1}{2} [\hat{\epsilon}_{Pb}(1-3\theta_{Pb}) + \hat{\epsilon}_s(3\theta_{Pb} - 2)] \quad (3)$$

$$\hat{B} = -\frac{1}{2} [\hat{\epsilon}_{Pb} \hat{\epsilon}_s] \quad (4)$$

$$\hat{n}_f = \hat{\epsilon}_f^{1/2} \quad (5)$$

The root with the largest modulus was used as solution of Eq. 1 (23).

The third layer represents dendritic Pb islands, visible in scanning electron micrographs, and was modeled by an island film and coherent superposition of polarization states (Eq. 6) resulting from reflection on adjacent surface elements with and without island coverage.

$$\hat{r}_v = \theta_f \hat{r}_{v,f} + (1-\theta_f) \hat{r}_{v,s} \quad (6)$$

Use of coherent superposition implies that the diameter of islands is smaller than the spacial coherence of the illuminating light. The total amount of Pb contained in the three layers was adjusted to agree with the coulometric measurements.

Although the three-layer model provides very good agreement between predictions and measurements, the computations have shown that the optical effect of the third (dendritic island) layer is often negligible, because the surface coverage by islands is small (5-10%). A simplified two-layer model was therefore used for interpretations. Only 3 unknown parameters have to be determined with this model (thickness of the first, compact layer, thickness and porosity of the second, porous layer) as opposed to six parameters required for the three-layer model. Despite the insignificant optical effect of the dendritic island layer, it usually contained about 2/3 of the Pb deposit known to be present from coulometric measurement. All optical constants were determined experimentally from independent measurements, and were not treated as adjustable parameters.

#### 4. Optimization of the Two-Layer Model

Optimized values of the wavelength-independent parameters of the two-layer model (thicknesses and porosity) were obtained by minimizing the sum-of-squares error between measurements and model predictions over the entire spectral range. As outlined in a previous paper (22) parameter

confidence intervals are calculated from the variance of the measurements by use of the student t-statistic at a 95% confidence level for "2N-P" degrees of freedom, where "N" is the number of delta-psi measurements over the spectral range (from a single spectroscopic scan) and "P" is the number of adjustable parameters. Wavelengths of individual measurements are spaced at intervals greater than the source bandwidth; measurements at each wavelength are treated as independent observations of the same surface.

Optimization of the wavelength-independent parameters required to specify only the first two layers resulted in smaller parameter variances than if all three layers were included, because the variance for any parameter increases dramatically as the total number of model parameters P approaches the number of data points (2N) used in the optimization. This strategy is based on the results of optical computations which had shown that the third (island) layer has an insignificant optical effect. All deposited Pb not accounted for in the first two layers after optimization was assumed to be contained in the dendritic islands.

Results of the optimization are shown in Figs. 5 and 6 (delta and psi vs. wavelength). The solid lines represent experimental measurements and the circles represent points calculated by a multidimensional optimization routine. Very good agreement was obtained by optimization of the thickness and porosity of the second layer, which are wavelength-independent adjustable parameters. Table II summarizes the results of the optimization. Measured and calculated values of delta and psi at

particular wavelengths are tabulated for three thicknesses. The amount of material, based on coulometric measurements, present in these films corresponds to compact layers of thickness 31, 60 and 110 nm. By minimizing the sum-of-squares error (24) between the model predictions and measured values of  $\delta$  and  $\psi$  over the entire spectral range, one determines the optimum values of the wavelength-independent adjustable parameters (thickness and porosity). Table II shows the values of the thickness and porosity of the porous layer with their statistically-determined confidence interval and the thickness of the compact layer which corresponds to that of the underpotential deposits (19,22). Thicknesses and porosities of the second layer are thus found to be 31 nm and 41 percent; 50 nm and 22 percent; and 87 nm and 3 percent, respectively.

The large error limits given for the film thickness in the last column of Table II ( $87 \pm 266$  nm) are caused by the fact that a layer of that thickness is just barely penetrated by the light (conventional penetration depth for normal incidence 8 and 13 nm at wavelength 400 and 700 nm, respectively) and behaves optically almost like bulk lead. The measurements are therefore insensitive to deposit thickness, resulting in a wide confidence interval.

#### IV. Inhibitor Effects

Conclusions about the effect of Rhodamine-B on deposit porosity were derived from spectroscopic ellipsometer measurements by the methods discussed in the preceding section. Figures 7 and 8 show, for a thin deposit (31 nm, based on charge), how the distinctive spectral properties of the Cu substrate, which are still visible through the deposit obtained without dye, were completely masked by a deposit of equal lead content obtained in the presence of the dye. The large optical difference is due to differences in porosity (45% without dye, <10% with dye). Spectral scans of  $\Delta$  for a thicker deposit (110 nm, based on charge) are shown in Fig. 9. Here, deposits made with and without Rhodamine-B show similar optical characteristics which can be interpreted as Pb layers too thick to be penetrated by the light, even for deposits obtained without dye. The optical interpretations were similar for deposits obtained with constant or cycling potential. The underpotential deposit can be represented as a compact monolayer in the absence of the dye and an incomplete monolayer in its presence.

The scanning electron micrographs shown in Fig. 10 illustrate the fine-grained initial (1 min, corresponding to 30 nm compact thickness) deposit obtained with the dye and the dendritic islands obtained without it. At a later stage of deposition (8 min, corresponding to 110 nm compact thickness) the effect of the dye begins to wear off and patches of porous deposit appear, while without dye the dendrites continue to grow into a matted layer.

Energy dispersive x-ray analysis has shown that the dendrites are composed of lead and that without dye the deposit between dendrites is very thin while it is thick and uniform with the dye, as had been inferred from the ellipsometer measurements.

#### V. Ellipsometry and Cyclic Voltammetry

Cyclic voltammetry and ellipsometry measurements (at 550 nm wavelength) were conducted simultaneously. A potential ramp (+100 to -800 mV vs. 4 M Ag/AgCl reference, 2.8 V/min) and current response are shown in Fig. 11. The corresponding ellipsometer measurements are given in Fig. 12. They show a response which coincides with the onset of a cathodic deposition current (points A and D for first and second sweep). The deposit thickness and porosity ( $1 - \theta_{pb}$ ) were determined by fitting the ellipsometer measurements to the two-layer optical model discussed in Section III.

Interpretations for selected measured points A-B, Figs. 11 and 12 are given in Table I. It can be seen that during the first potential cycle the presence of the dye results in a higher volume fraction (lower porosity) of lead in the bulk deposit. The effect of the dye gradually disappears in the second and subsequent cycles, where volume fractions close to those without dye are obtained (22). Thus, a 15% porosity obtained in the first potential sweep for a layer of 29.6 nm thickness compares to a 34% porosity obtained in the second sweep at 42 nm thickness. This increase in porosity is responsible for the change from a positive to a negative response in  $\Delta$  to deposition between the first and subsequent sweeps. Depletion of dye at the electrode surface is the

cause for this change in behavior. The effect of Rhodamine-B on deposit porosity reappears after relaxation periods at open circuit. The optical constants of compact lead ( $\hat{n} = 2.1 - 4.2 i$ ) were combined with the refractive index of the electrolyte ( $n = 1.34$ ) to compute the optical properties of the porous deposits by use of the Bruggeman equation. The optical constants of the copper substrate were measured as  $\hat{n} = 0.7 - 3.4 i$ .

The amount of lead in the bulk deposit derived from the ellipsometer measurements (product of thickness  $d$  and volume fraction  $\theta_{pb}$ ) is always less than the amount based on the charge passed (thickness  $d_q$ ), as shown in the last column of Table I. The ratio is lower for deposits without dye; in agreement with the formation of more dendritic islands, which are not measured optically (2).

## VI. Measurement of the Inhibitor Layer

Underpotential and bulk peaks in the cyclic voltammograms are shifted to more cathodic potentials by adsorbed Rhodamine-B. Due to depletion of the dye, this potential shift disappears, however, after several uninterrupted potential cycles, but it reappears after relaxation periods (10 to 60 min) at open circuit, during which adsorption can take place by diffusion from the electrolyte (Fig. 13). The repopulation of the electrode surface with Rhodamine-B adsorbate has also been observed by spectroscopic ellipsometry; differential measurements with and without dye (Figs. 14 and 15) show the development of spectral features due to the adsorbed dye. These spectral scans were taken immediately preceding the corresponding cyclic voltammograms of Fig. 13, the relaxation times

in minutes are indicated along the curves. A study of the adsorbed dye layer (25) which will be presented elsewhere, has shown that molecules oriented normal to the electrode surface, forming an adsorbate layer of 32 Å thickness, appear to be responsible for the inhibition of Pb deposition.

The long relaxation times required to restore Rhodamine-B coverage of the surface are due to the slow diffusion from the very dilute (10 μM) solution (26). For a coverage between  $4 \times 10^{13}$  and  $2 \times 10^{14}$  molecules/cm<sup>2</sup>, assuming a linear adsorption isotherm with an equilibrium constant of 0.01 to 0.03 cm (27), a 30 minute time to half-coverage would require a diffusion coefficient between  $5.6 \times 10^{-8}$  and  $5.0 \times 10^{-7}$  cm<sup>2</sup>s<sup>-1</sup>, which appears reasonable.

## VII. Conclusions

Rhodamine-B acts as a deposition inhibitor for the electrodeposition of Pb on Cu and Ag. Potentials required for deposition are more cathodic in the presence of Rhodamine-B than in its absence.

Less porous deposits are formed in the presence of the dye and the underpotential deposit is less than a complete monolayer. The observed decrease in bulk deposit porosity resulting from the addition of Rhodamine-B can be attributed to an increase in nucleation density on the surface and inhibition of dendrite growth.

If nucleation of the bulk deposit is favored at imperfections of the first monolayer of the underpotential deposit, the partial monolayer formed in the presence of Rhodamine-B may provide a higher density of nucleation sites. Also, because deposition occurs at more cathodic potentials in the presence of the dye, the equilibrium size of nuclei on the surface is

smaller and their number larger. Kinetic effects of the adsorbed dye molecules may involve a decrease in the surface diffusion of Pb adatoms which would also result in a higher nucleation density.

The selective reduction of Rhodamine-B at easily accessible (high activity) sites, such as tips of dendrites, in favor of  $Pb^{++}$  reduction, could shift the deposition to less accessible sites close to the surface which would preferentially be supplied by  $Pb^{++}$  because of its higher diffusion coefficient.

The dye is reduced at the surface and inhibitory effects on the deposit micromorphology disappear until the surface is repopulated with adsorbate during relaxation periods at open circuit.

Spectroscopic ellipsometry allows one to calculate confidence intervals of wavelength-independent parameters for micromorphological optical models and to justify the use of more sophisticated optical models on the basis of the greater degrees-of-freedom.

For three electrolytically formed Pb deposits (compact thickness 31 nm, 60 nm, and 110 nm) the best agreement between measurements and model predictions was obtained for a three-layer model or a two-layer simplification of it. The distribution of deposited material between compact, porous (granular), and dendritic island layers could be determined.

#### Acknowledgment

This work was supported by the Director, Office of Energy Research, Office of Basic Energy Sciences, Materials Sciences Division of the U.S. Department of Energy under contract no. DE-AC03-76SF00098. This was paper 822 presented at the San Francisco, California, meeting of the Society, May 8-13, 1983.

NOMENCLATURE

d	thickness of deposit derived from ellipsometer measurements
$d_q$	thickness of deposit for a compact layer, based on charge
k	imaginary part of complex refractive index
n	real part of complex refractive index
$\hat{n}_f$	complex refractive index of porous film
$\hat{n}_s$	complex refractive index of substrate
$\hat{r}_v$	complex Fresnel reflection coefficient for polarization v (s or p)
$\hat{r}_{v,f}$	complex Fresnel reflection coefficient for film-covered surface
$\hat{r}_{v,s}$	complex Fresnel reflection coefficient for bare surface
$\hat{A}, \hat{B}$	complex parameters for quadratic equation
E	Potential vs. 4M Ag/AgCl
N	number of pairs of $\Delta$ and $\psi$ measurements
P	number of model parameters to be fitted
Q	charge passed
$\alpha$	level of confidence, $1-2\alpha$
$\hat{\epsilon}_f$	complex dielectric function of porous film
$\hat{\epsilon}_{Pb}$	complex dielectric function of metallic Pb
$\hat{\epsilon}_s$	complex dielectric function of electrolyte solution
$\theta_f$	fraction of surface covered by film of refractive index $\hat{n}_f$

$\theta_{Pb}$	volume fraction of Pb in porous film derived from ellipsometer measurements
$\Delta$	ellipsometer parameter, phase difference between p and s electric field components after reflection, relative to the incident (degrees)
$\Delta_C$	calculated value of $\Delta$
$\Delta_M$	measured value of $\Delta$
$\psi$	ellipsometer parameter, amplitude ratio of p and s electric field components after reflection ( $\tan \psi$ ), relative to the incident (degrees)
$\psi_C$	calculated value of $\psi$
$\psi_M$	measured value of $\psi$

## References

1. J. A. Harrison, and H. R. Thirsk, in Electroanalytical Chemistry, Vol. 5, edited by A. J. Bard, Marcel Dekker, New York, 1971
2. R. H. Muller and J. C. Farmer, *J. de Phys.* 44, C10 (1983).
3. R. H. Muller and J. C. Farmer, *Rev. Sci. Instrum.* 55, 371 (1984).
4. G. Hass and L. Hadley, in American Institute of Physics Handbook, 2nd ed., edited by D. E. Gray, McGraw Hill, New York, 1963.
5. P. B. Johnson and R. W. Christy, *Phys. Rev. B* 6, 4370 (1972).
6. D. M. Kolb and R. Kötz, *Surf. Sci.*, 64, 698 (1977).
7. P. Bousquet, *J. Phys. Rad.*, 21, 873 (1960).
8. J. B. Birks, Photophysics of Aromatic Molecules, Wiley, London, 1970.
9. W. J. Plieth, P. Gruschinske, and H. J. Hensel, *Ber. Bunsenges. Phys. Chem.* 82, 615 (1978).
10. S. Schmidt and R. Reich, *Ber. Bunsenges. Phys. Chem.* 76, 599 (1972).
11. M. Pourbaix, Atlas of Electrochemical Equilibria in Aqueous Solutions, Pergamon Press, New York, 1966.
12. D. M. Kolb, in Advances in Electrochemistry and Electrochemical Engineering, edited by H. Gerischer and C. W. Tobias, Vol. 11, Wiley, New York, 1978.
13. D. E. Aspnes, J. B. Theeten and F. Hottier, *Phys. Rev. B*, 20, 3292 (1979).
14. R. M. A. Azzam and N. M. Bashara, *Phys. Rev. B* 5, 4721 (1972)
15. R. H. Muller and C. G. Smith, *Surf. Sci.*, 96, 375 (1980).
16. D. E. Aspnes and J. B. Theeten, *Phys. Rev. B* 20, 3292 (1979).
17. R. H. Muller in Advances in Electrochemistry and Electrochemical Engineering, Vol. 9, edited by C. W. Tobias and P. Delahay, Wiley, New York, 1973, p. 220.

18. C. G. Smith, Ph.D Thesis, Department of Chemical Engineering, University of California, Berkeley, LBL-8082 (1978).
19. R. H. Muller and J. C. Farmer, Surf. Sci., 135, 521 (1983).
20. G. R. Fowles, Introduction to Modern Optics, 2nd ed., Holt, Rinehart, and Winston, New York, 1975, p. 74.
21. M. Born and E. Wolf, Principles of Optics, 2nd ed. MacMillan, New York, 1964, p. 551.
22. J. C. Farmer and R. H. Muller, Electrochem. Soc. Meeting, San Francisco, CA, May 8-13, 1983. Ext. Abstr. 823, submitted to J. Electrochem. Soc.
23. W. Kahan, personal communication, Department of Electrical Engineering and Computer Science, University of California, Berkeley, August 1982.
24. G. E. Box and G. A. Coutie, Proc. Inst. Electr. Engrs., 103 B, Suppl. 1, 100 (1956).
25. J. C. Farmer, Ph.D dissertation, Department of Chemical Engineering, University of California, Berkeley, LBL-15607, (March 1983).
26. T. K. Sherwood, R. L. Pigford and C. R. Wilkie, Mass Transfer, McGraw-Hill, New York, 1975, p. 34.
27. A. J. Bard and L. R. Faulkner, Electrochemical Methods, Fundamentals and Applications, Wiley, New York, 1980, p. 518-519.

Table I. Effect of Rhodamine-B on the morphology of Bulk Pb Deposits during cyclic voltammetry. Comparison of thickness  $d_q$  of bulk deposit derived from charge passed with thickness  $d$  and volume fraction  $\theta_{pb}$  obtained from ellipsometer measurements. Points B to F selected in first and second potential sweep identified in Figs. 11 and 12.

Sweep No, Point	E (mV)	$d_q$ (nm)	$d$ (nm)	$\theta_{pb}$	$\frac{dx\theta_{pb}}{d_q} \times 100(\%)$
NO DYE ADDED					
1, B	-582	16.3	7.5	0.38	17
1, C	-430	37.9	50.6	0.56	75
2, B	-573	16.3	8.6	0.35	18
2, C	-400	37.9	50.9	0.55	74
10 $\mu$ M RHODAMINE-B					
1, B	-800	21.7	11.3	0.89	46
1, C	-439	37.9	29.6	0.85	66
2, B	-800	27.1	24.4	0.61	55
2, C	-388	43.3	42.0	0.66	64

Table II. Spectroscopic Ellipsometry of Pb Deposits: Optimization of 2-Layer Model. Confidence Intervals for Model Parameters given for 95% Confidence Limits.

Thickness of Compact Deposit $d_c$ based on charge	30 nm	60 nm	110 nm
THICKNESS OF POROUS LAYER (nm)	$31 \pm 4.1$	$50 \pm 16.2$	$87 \pm 266.4$
VOL. FRACTION Pb IN POROUS LAYER	$0.585 \pm 0.139$	$0.775 \pm 0.165$	$0.968 \pm 0.274$
THICKNESS OF COMPACT (UPD) LAYER (nm)	$0.48 \pm 0.11$	$0.48 \pm 0.11$	$0.48 \pm 0.11$

Figure Captions

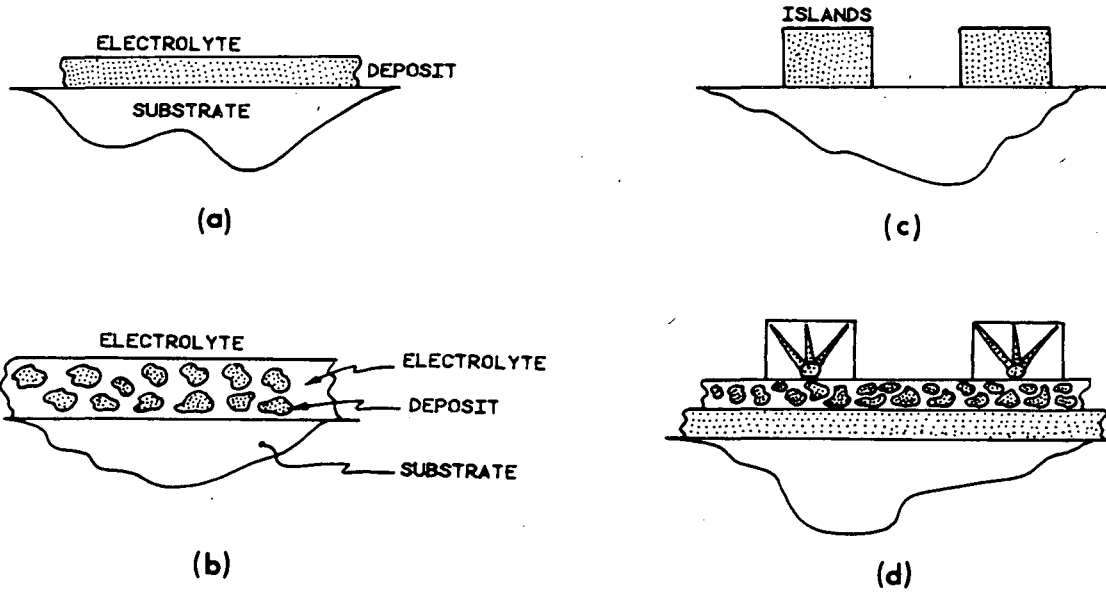
Fig. 1. Schematic of film models investigated for the interpretation of spectroscopic ellipsometer measurements of thin Pb deposits on Cu substrates. Number of adjustable parameters given in parentheses. (a) compact single film (1); (b) porous single film, optical constants of effective medium determined according to Maxwell-Garnett (2) or Bruggeman (2); (c) island single film, reflection coefficient determined by coherent superposition of polarization states, islands compact (2), porous (3) or anisotropic (6); (d) multilayer films, three layers: compact and porous layers, dendritic islands (6) or two layers: compact and porous films (3).

Fig. 2. Spectroscopic simulations for compact film model (solid lines). Pb deposits of thickness 0, 1, 5, 10, 20, 31, 60, 110 nm. Experimental measurements (dotted lines) for 31, 60, 110 nm equivalent compact Pb deposits ( $d_q$ , based upon coulometric measurements) on Cu.

Fig. 3. Spectroscopic simulations of porous film model (solid lines). Volume fractions of Pb 0.1 to 0.9, amount of deposit corresponding to a 31 nm compact Pb layer on a Cu substrate. Simulations based upon the effective medium approximation (Bruggeman eq.). Experimental measurements (dotted lines) for 0 and 31 nm equivalent compact film.

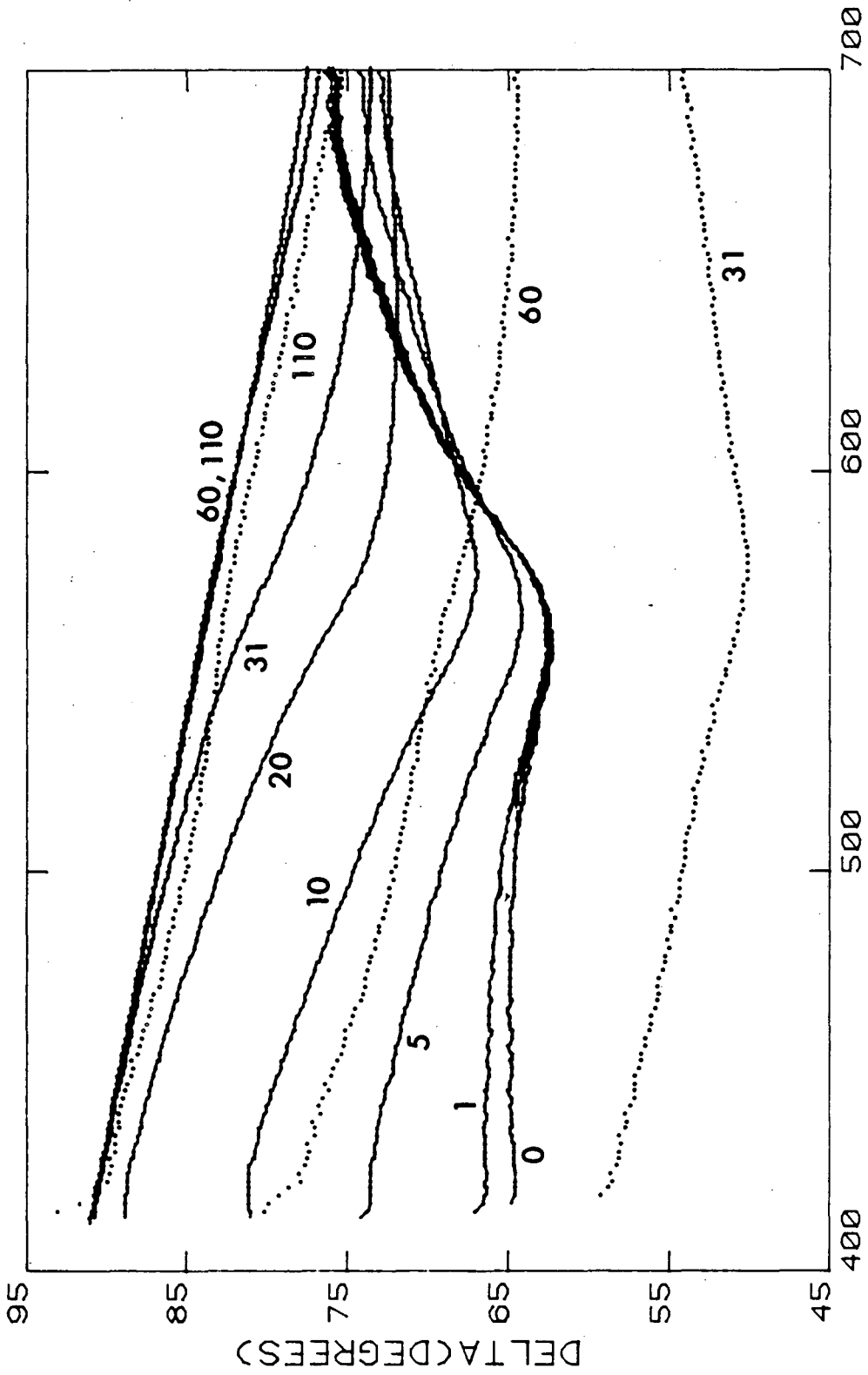
- Fig. 4. Spectroscopic simulations of island film model (solid lines). Surface coverage 0.1 to 1.0, amount of deposit corresponding to 31 nm compact layer, Cu substrate. Simulations based on coherent superposition of polarization states. Experimental measurements (dotted lines) for 0 and 31 nm equivalent compact film.
- Fig. 5. Spectroscopic simulation for optimum fit of ellipsometer parameter  $\delta$  for a two-layer film model (circles) and measurements (solid lines) for equivalent deposit thicknesses of 0, 31, 60 and 110 nm. Film parameters derived from optimum fit of model predictions to measurements given in Table II.
- Fig. 6. Spectroscopic simulation for optimum fit of ellipsometer parameter  $\psi$  for a two-layer film model; other comments as in Fig. 5.
- Fig. 7. Spectroscopic measurement of ellipsometer parameter  $\delta$  for thin Pb deposit on Cu (corresponding to 31 nm compact thickness); effect of presence of dye, bare Cu substrate shown for comparison. Potentiostatic deposition, -600 mV vs. Ag/AgCl, electrolyte as in Fig. 1, except for dye. Substrate visible through porous deposit obtained without dye.
- Fig. 8. Spectroscopic measurement of ellipsometer parameter  $\psi$ , data as for Fig. 7.
- Fig. 9. Spectroscopic measurement of ellipsometer parameter  $\delta$  for thick Pb deposit on Cu (corresponding to 110 nm compact thickness). Substrate obscured.

- Fig. 10. Effect of Rhodamine-B on the micromorphology of thin (1 min., 30 nm) and thick (8 min., 110 nm) Pb deposits; scanning electron micrographs. Potentiostatic deposition at -600 mV vs. Ag/AgCl.
- Fig. 11. Potential cycles (+100 to -800 mV vs. Ag/AgCl, sweep rate 2.8 V/min) applied to working electrode ( $1.13 \text{ cm}^2$ ) and resulting current response. Pb deposition on Cu from 5 mM  $\text{Pb}(\text{NO}_3)_2$ , 1 M  $\text{NaClO}_4$ , pH 3, 10 $\mu\text{M}$  Rhodamine-B. Evaluation of measurements at points B to F shown in Table I.
- Fig. 12. Ellipsometer measurements collected during potential cycles shown in Fig. 11; wavelength 550 nm (10 nm bandwidth), angle of incidence 75 deg.
- Fig. 13. Re-adsorption of Rhodamine-B on Cu during 5-60 min. relaxation at open circuit after removal by multiple potential sweeps; effect on cyclic voltammograms, 2 V/min, 1 M  $\text{NaClO}_4$ , 5 mM  $\text{Pb}^{++}$ , 10 $\mu\text{M}$  dye, pH 3,  $1.27 \text{ cm}^2$ .
- Fig. 14. Differential spectroscopic measurements of ellipsometer parameter  $\Delta$  for re-adsorption of Rhodamine-B on Cu after multiple potential sweeps. (Spectra for bare Cu in electrolyte without dye subtracted.) Relaxation periods at open circuit in minutes given along curves. Experimental conditions as in Fig. 13.
- Fig. 15. Differential spectroscopic measurements of ellipsometer parameter  $\psi$  for re-adsorption of Rhodamine-B on Cu. Experimental conditions as in Fig. 13.



XBL 829-11873 A

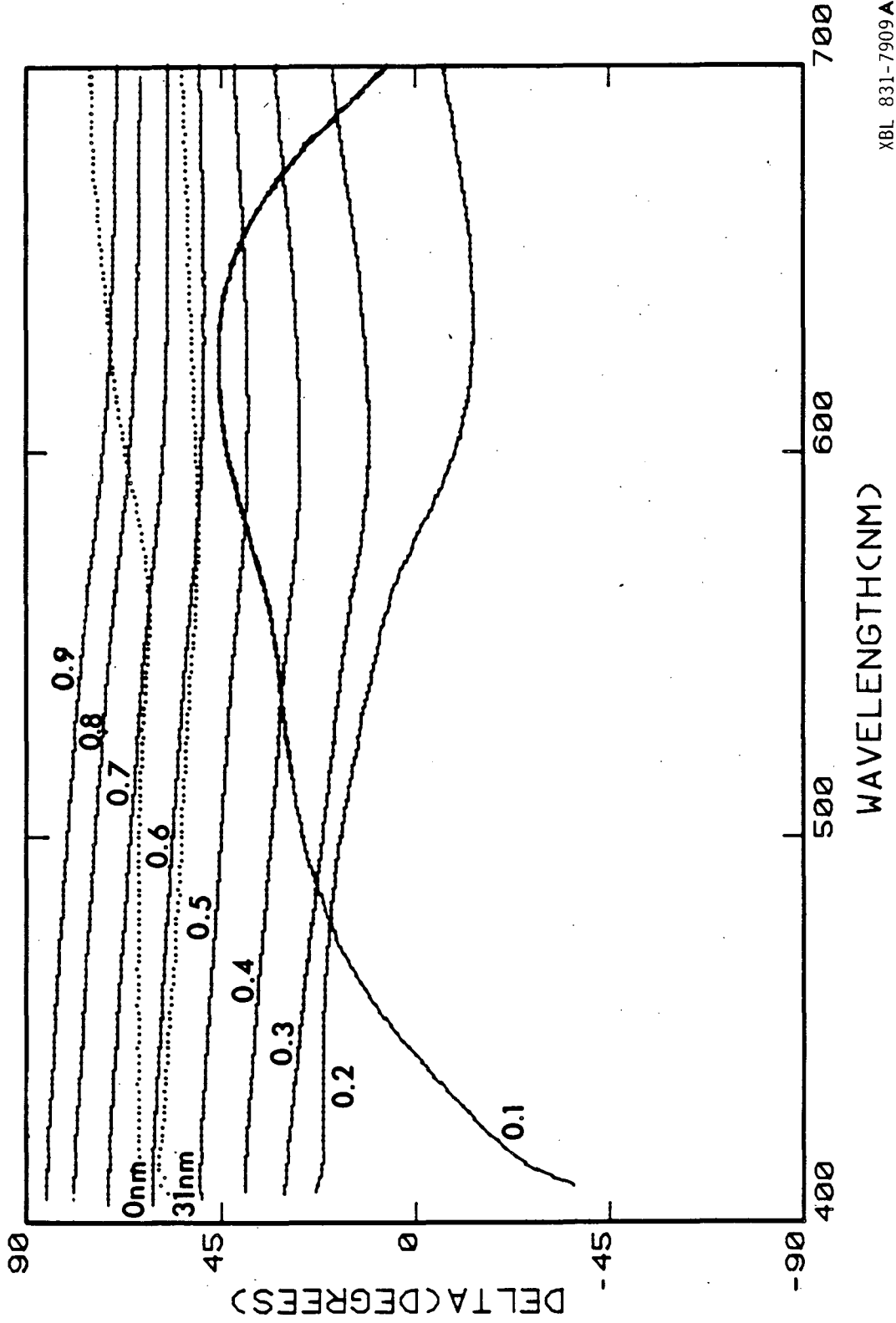
Fig. 1.



WAVELENGTH(NM)

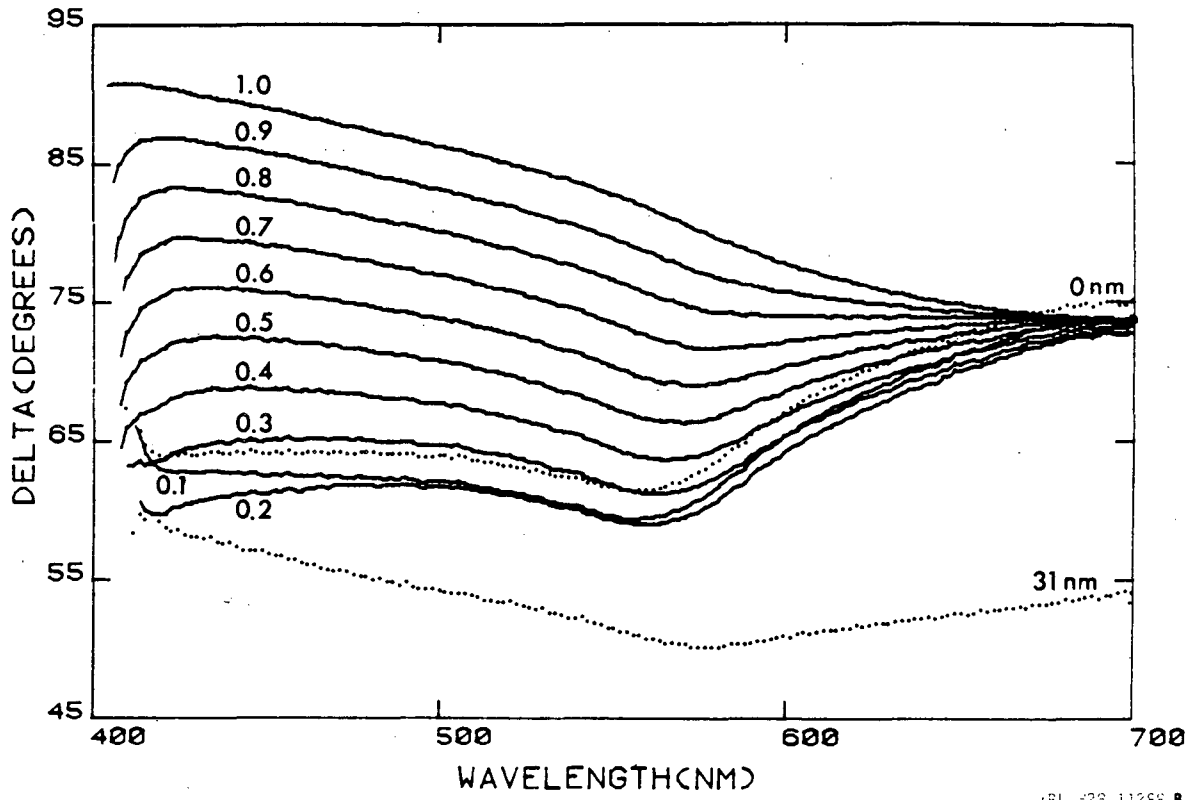
Fig. 2

XBL 828-11282A



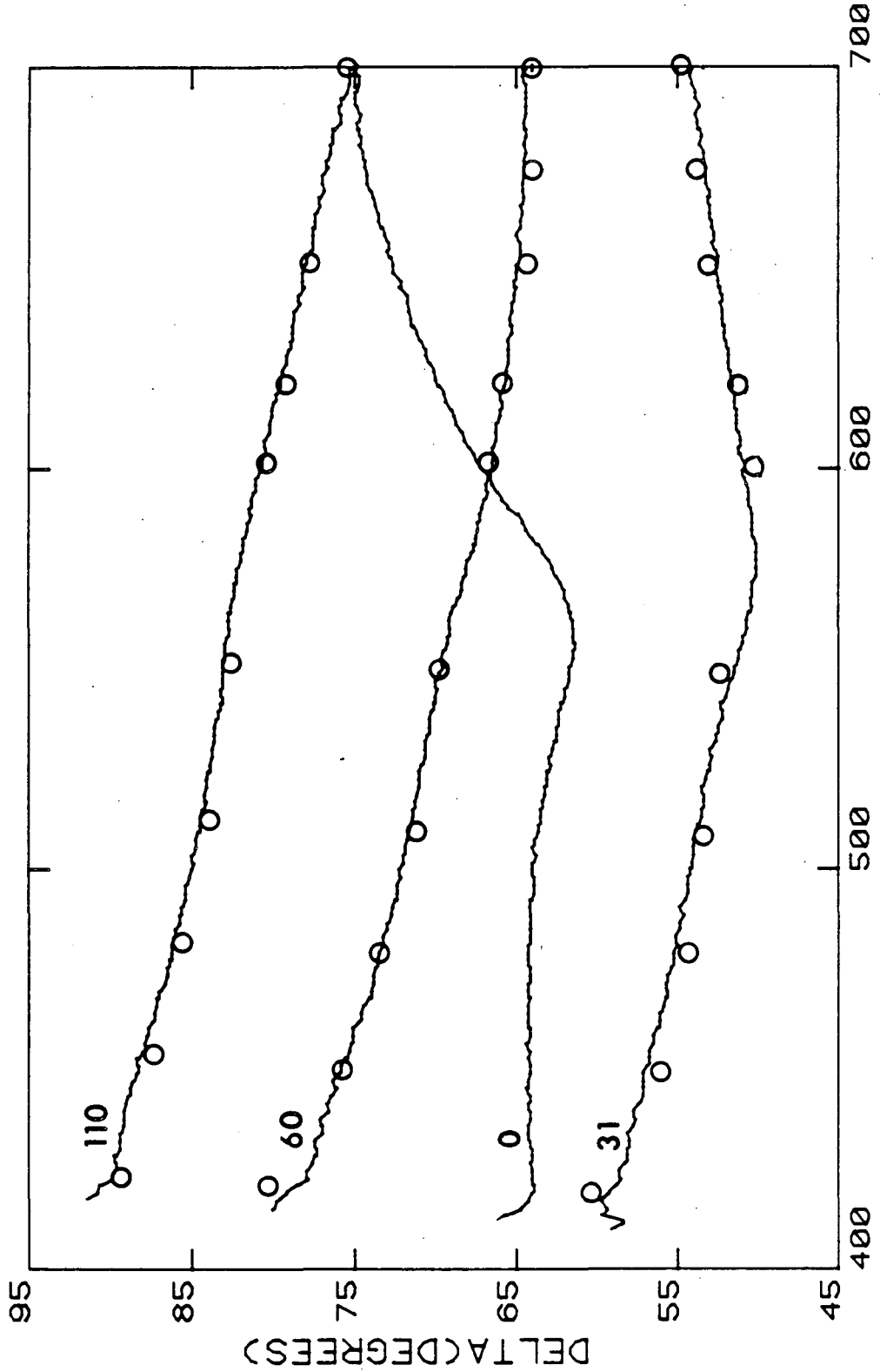
XBL 831-7909A

Fig. 3



BL 628-11288 B

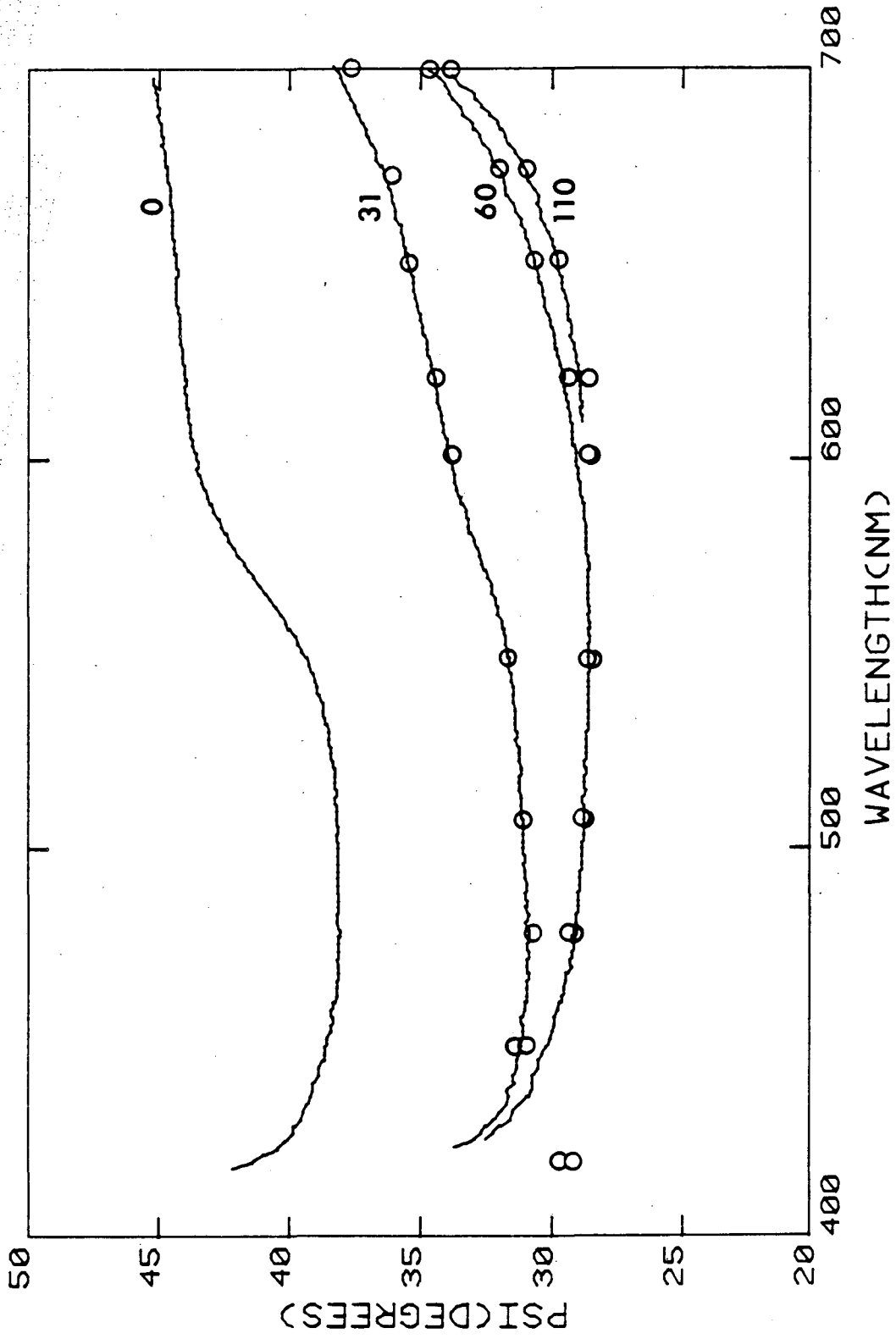
Fig. 4



XBL 831-7911A

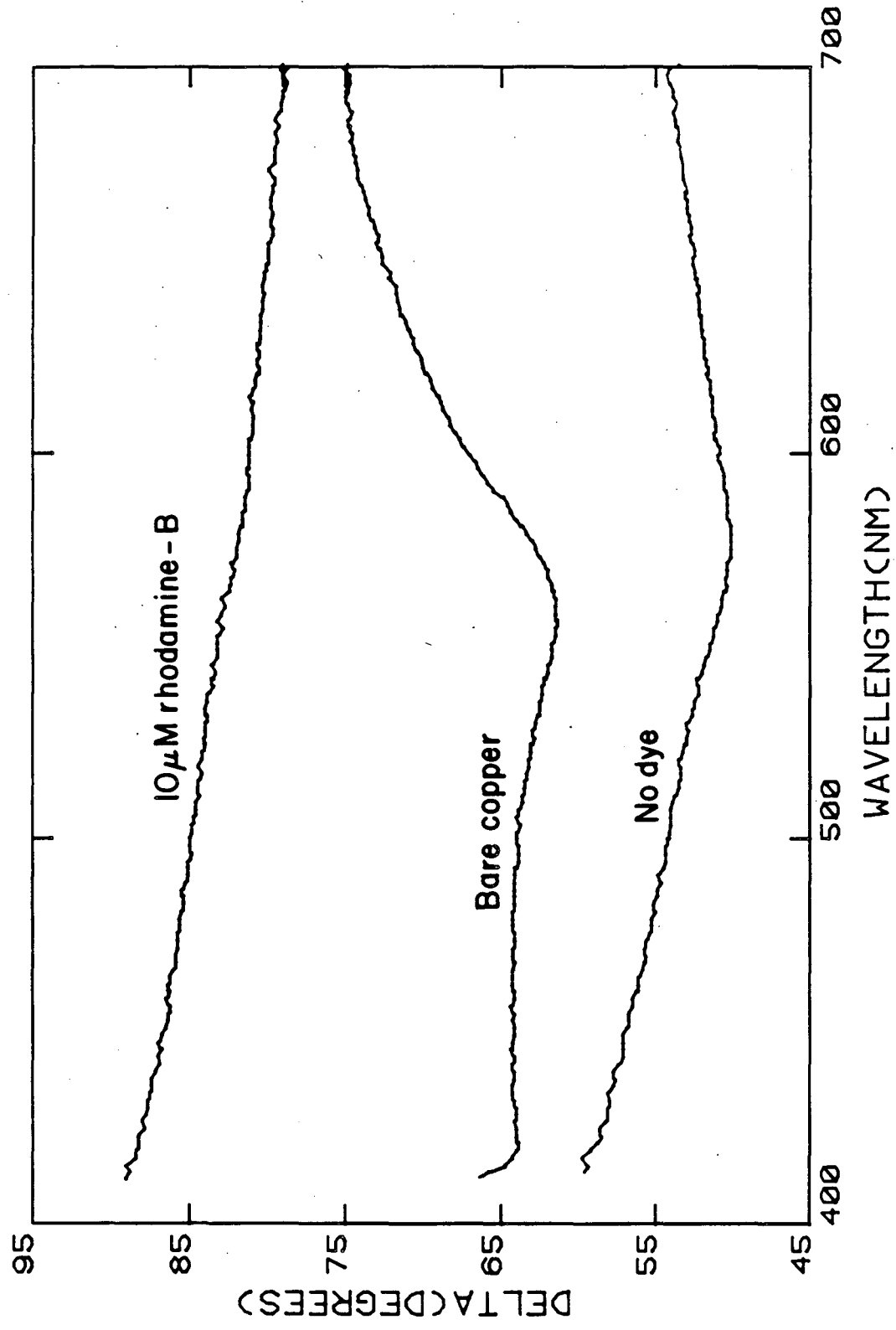
WAVELENGTH(NM)

Fig. 5



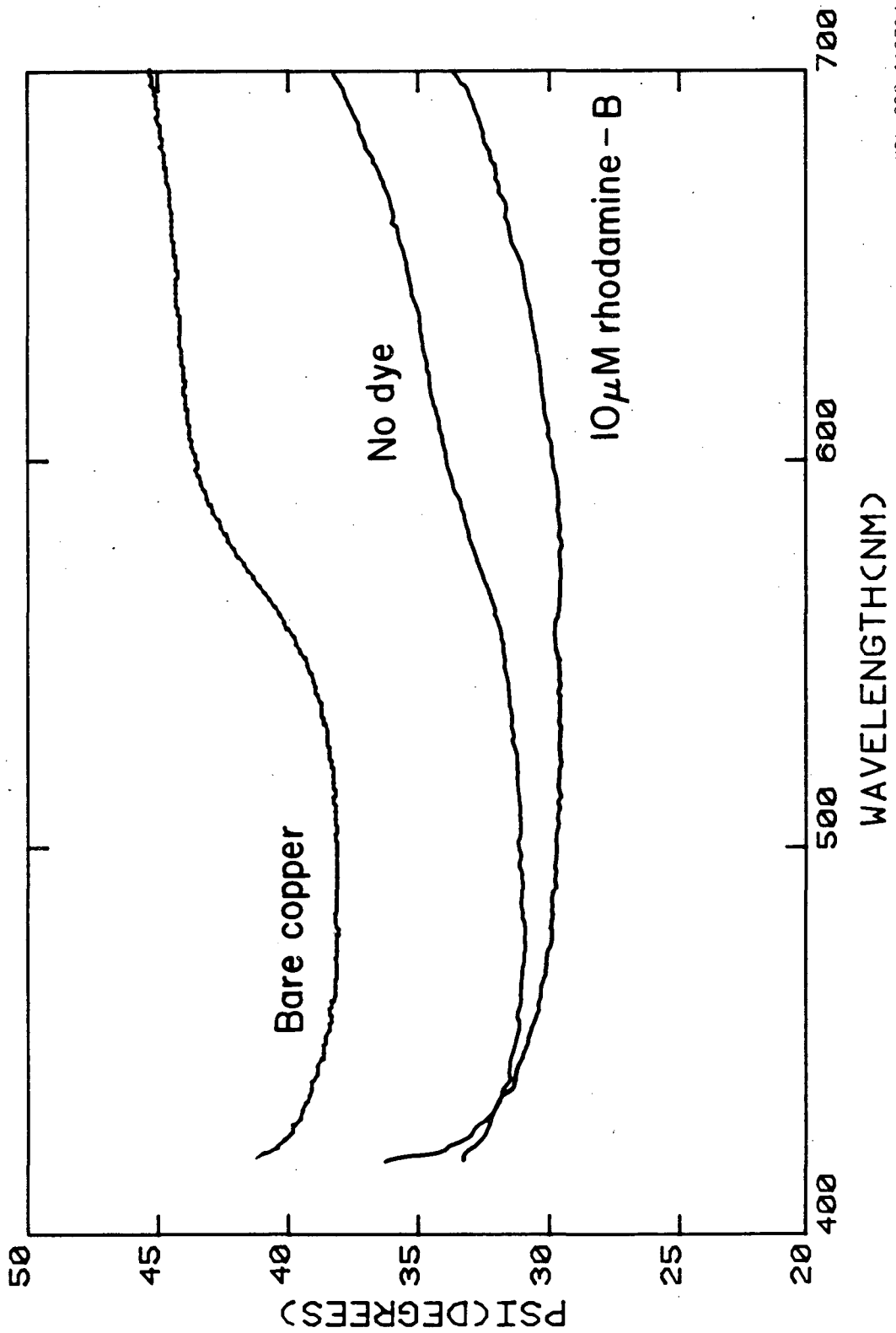
XBL 831-7912 A

Fig. 6



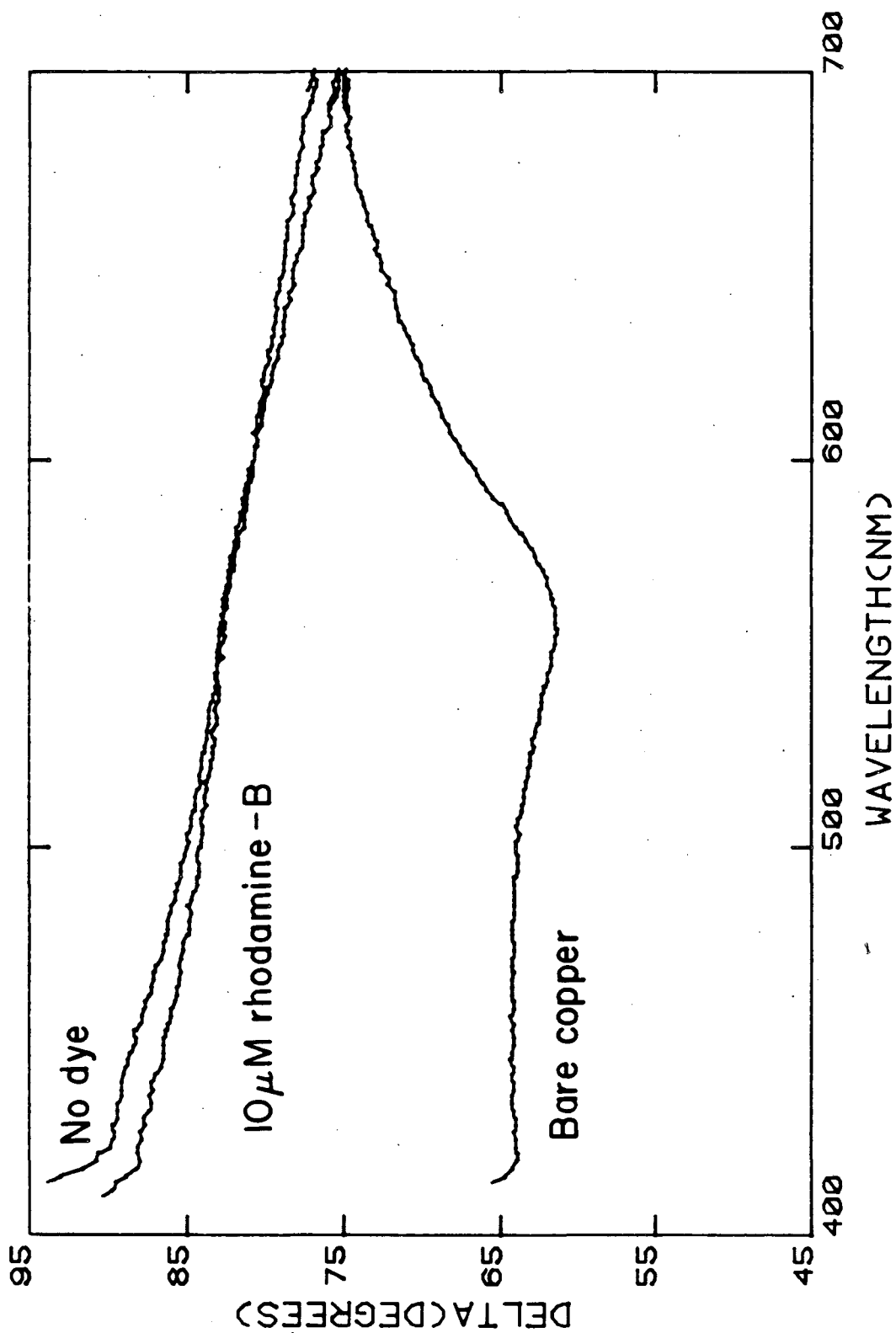
XBL 828-11272B

Fig. 7



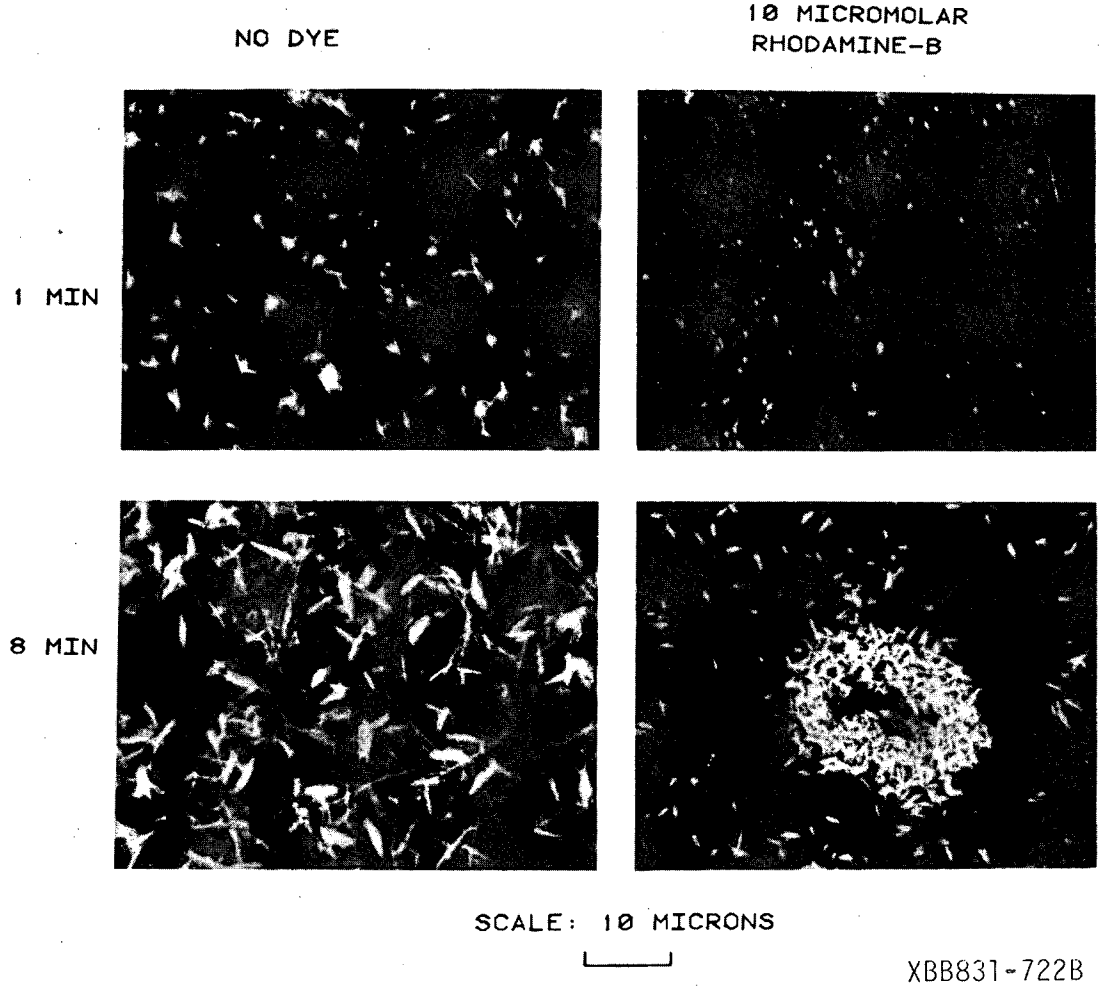
XBL 828-11273A

Fig. 8



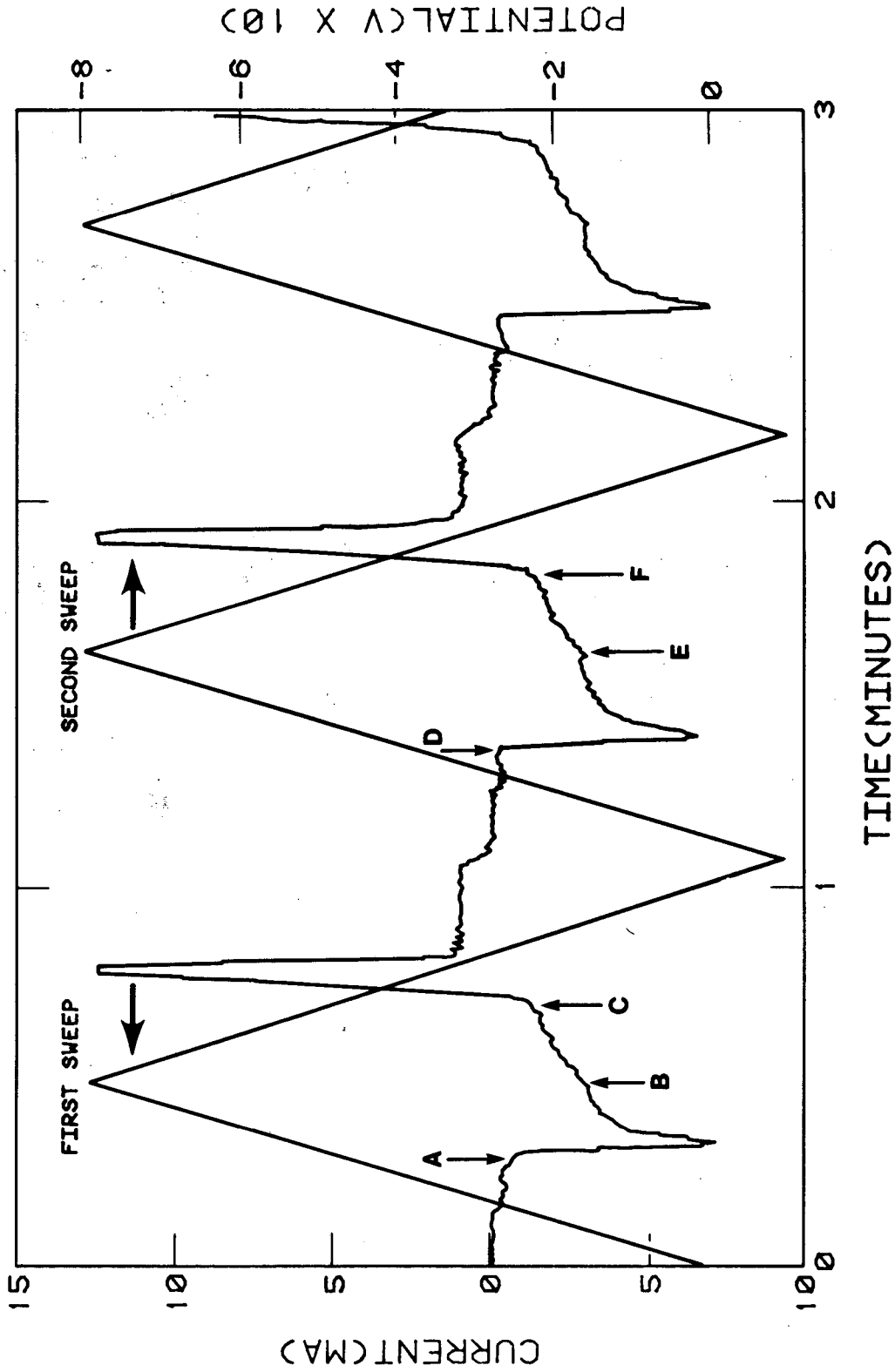
XBL 828-11276A

Fig. 9



XBB831-722B

Fig. 10



XBL 829-9655B

Fig. 11

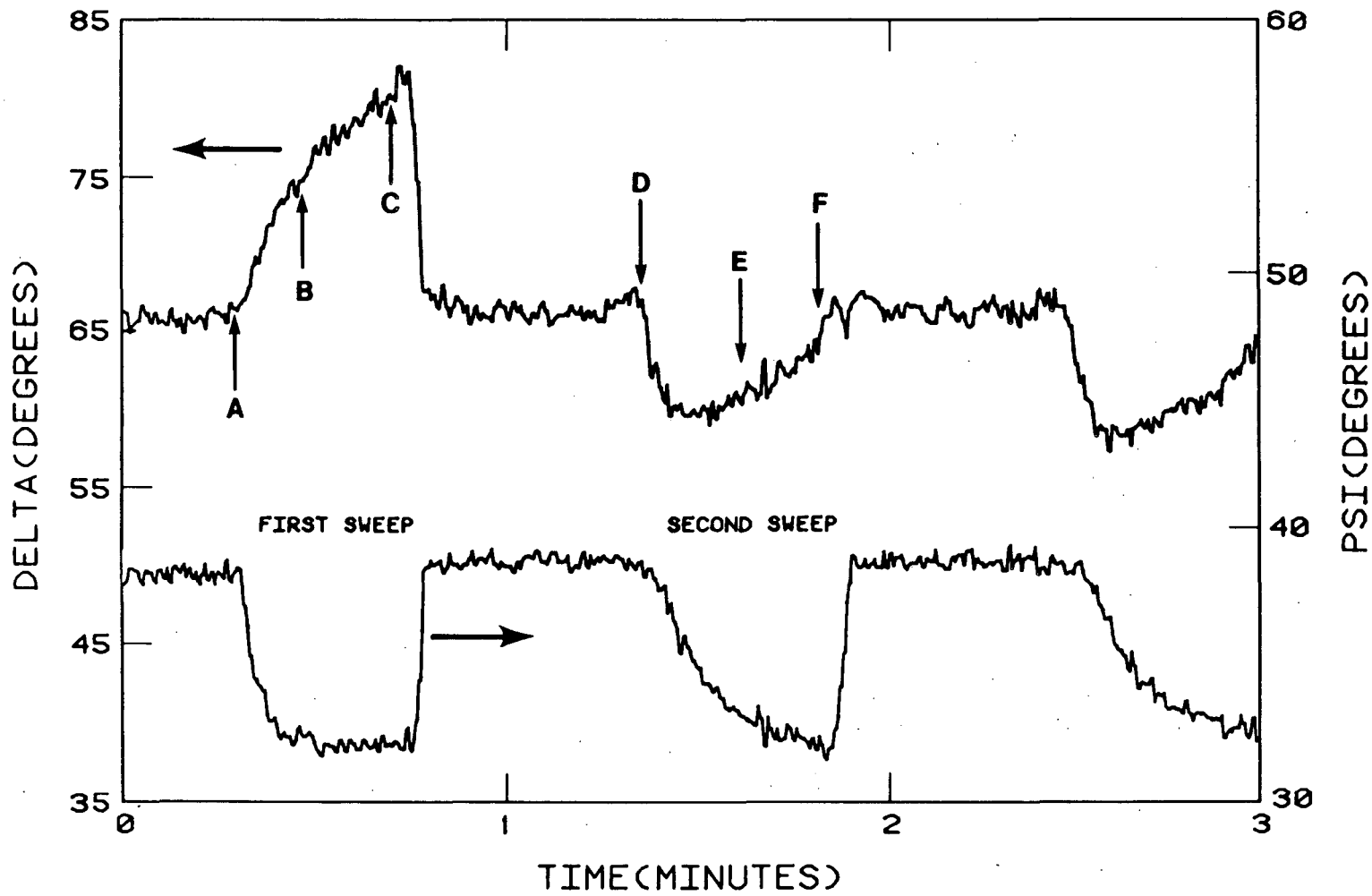
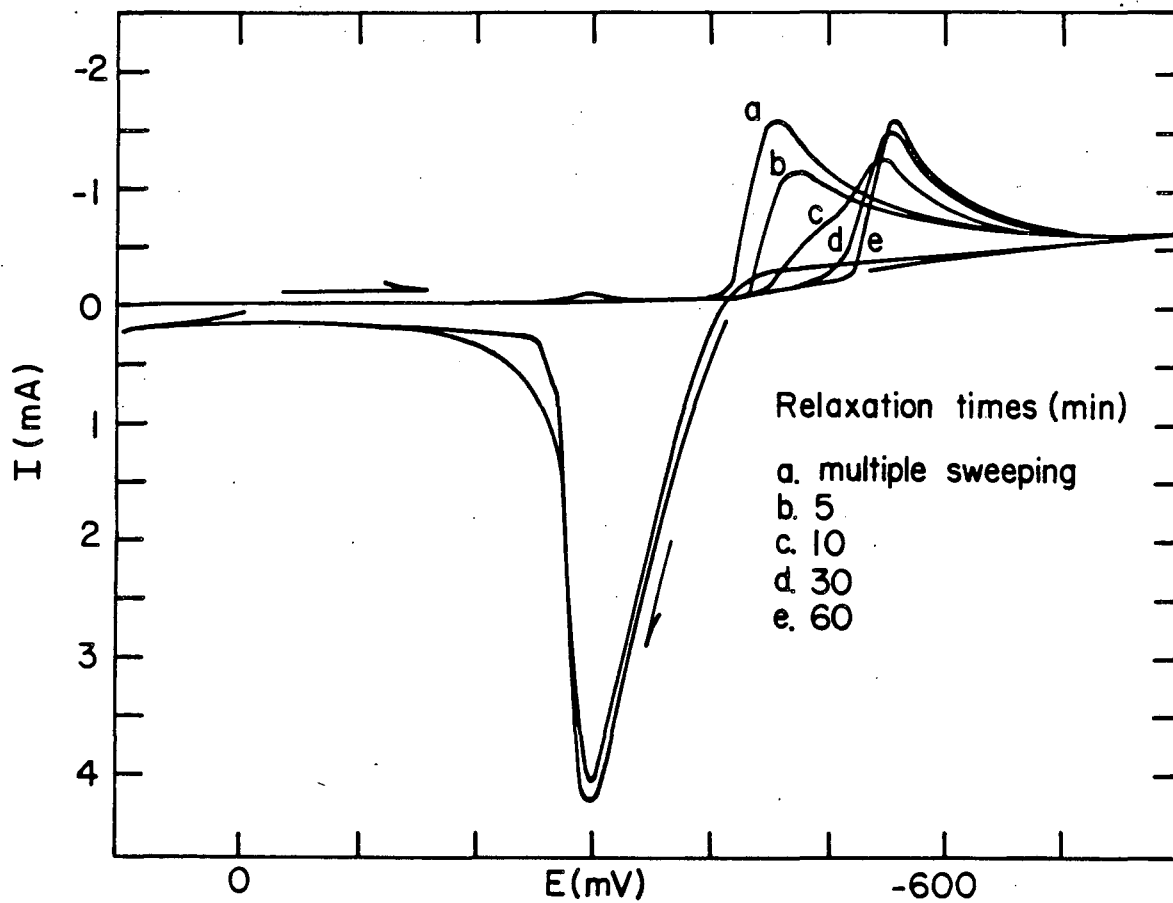


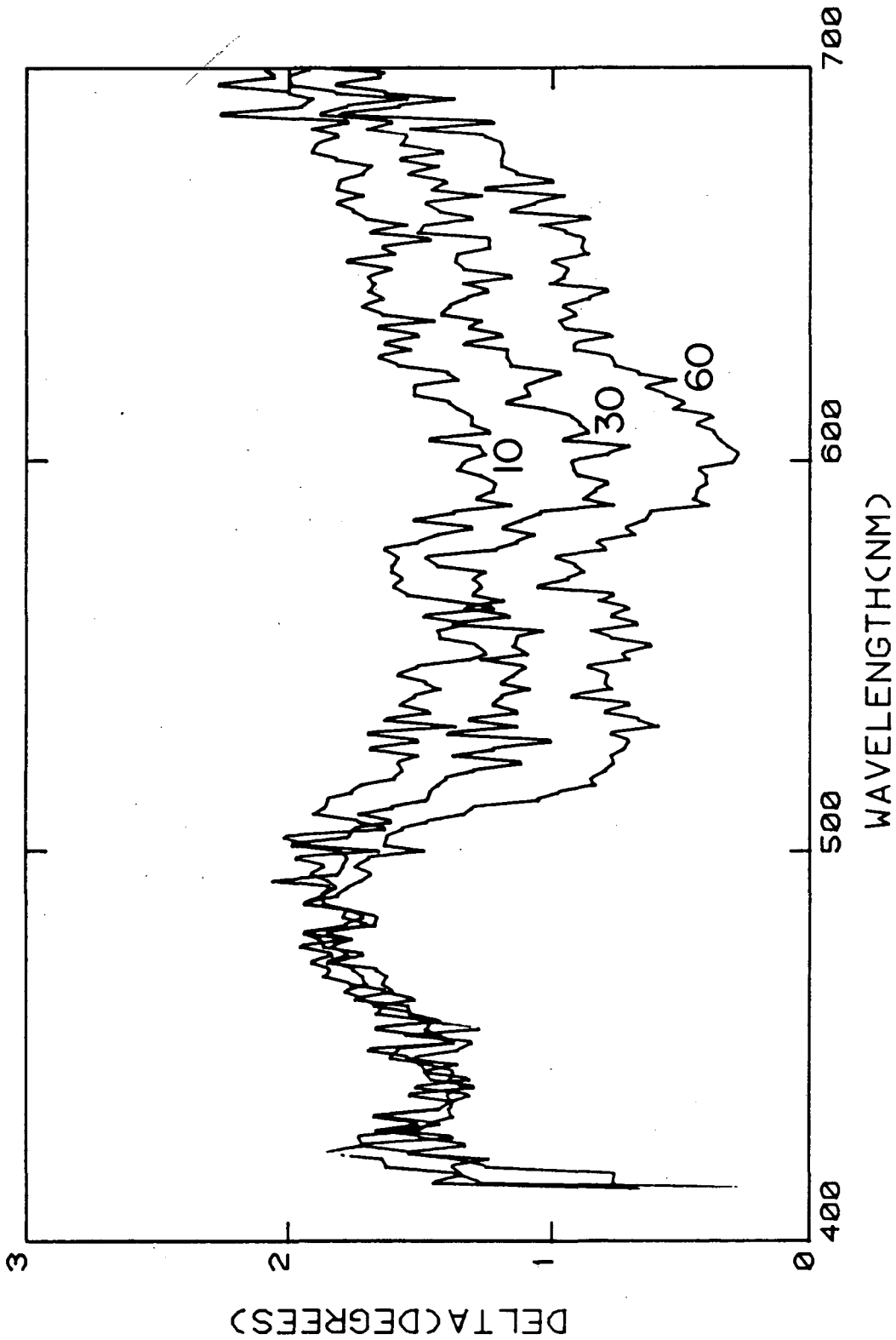
Fig. 12

XBL 829-9657B



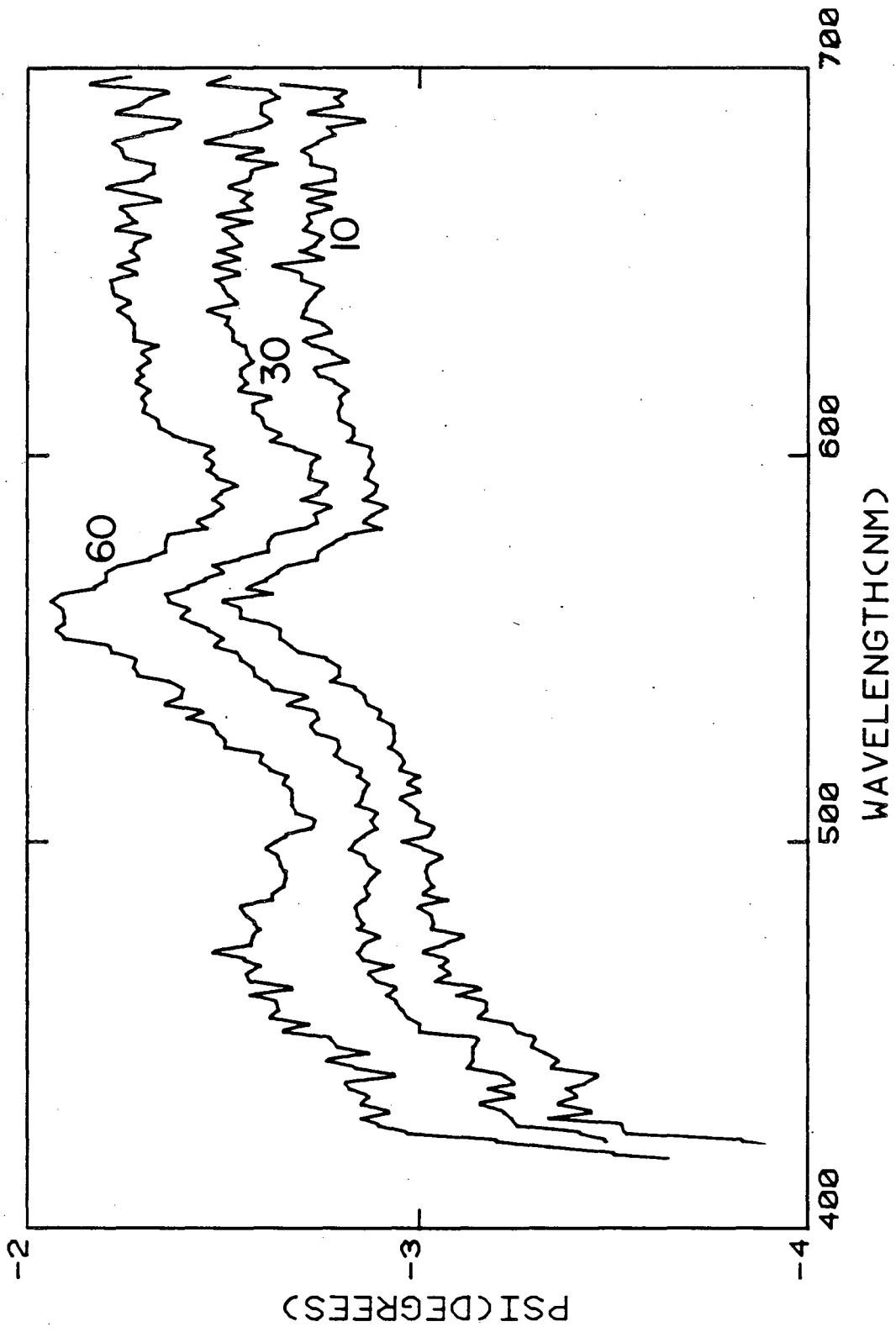
XBL 829-11598 A

Fig. 13



XBL 829-9660A

Fig. 14



XBL 829-9661A

Fig. 15

This report was done with support from the Department of Energy. Any conclusions or opinions expressed in this report represent solely those of the author(s) and not necessarily those of The Regents of the University of California, the Lawrence Berkeley Laboratory or the Department of Energy.

Reference to a company or product name does not imply approval or recommendation of the product by the University of California or the U.S. Department of Energy to the exclusion of others that may be suitable.

TECHNICAL INFORMATION DEPARTMENT  
LAWRENCE BERKELEY LABORATORY  
UNIVERSITY OF CALIFORNIA  
BERKELEY, CALIFORNIA 94720